Proceedings of The 2018 IEEE International
Conference on Real-time Computing and Robotics
August 1-5, 2018, Kandima, Maldives

Spiraling Motion of a Gliding Robotic Dolphin Based on the 3-D Dynamic Model

Jian Wang[1,2], Zhengxing Wu[2], Yueqi Yang[1,2], Min Tan[2], and Junzhi Yu[2]

Abstract— **This paper proposes a complete three-dimensional (3-D) dynamic model of a gliding robotic dolphin with full consideration of both 3-D gliding motion and flapping motion. The gliding robotic dolphin can not only implement an efficient dolphin-like swimming, but also has long endurance due to the buoyancy-driven system. Firstly, the mechanical structure including dolphin-like swimming part and gliding part of the robot is offered. More importantly, derivation processes of the kinematic analysis, net buoyancy analysis, hydrodynamic analysis, and multi-link dynamic modeling are discussed in detail to provide theoretical support. Furthermore, this paper presents some comparison of the spiraling movements based on these two different swimming motions, and gives the corresponding analyses according to the simulation results. Finally, through comparing results of the aquatic experiments and the simulation, we verify the complete dynamic model, and analyze the yaw angle and diving depth.**

I. Introduction

In recent years, aquatic biomimetics have attracted wide attention of researchers, especially in aspects of high adaptability and maneuverability for many underwater creatures [1]. As a kind of cetaceans, dolphins could perform many astonishing motions with their excellent natural advantages. They could easily achieve a swimming speed over 11 m/s, and perform high maneuverability, like a turn radius as small as 0.20 body lengths (i.e., BL) [2].

Fascinated by these excellent skills, more researchers have focused on robotic dolphins, which lead to great development in the last two decades [3]. Dogangil *et al.* presented some dynamic simulation studies and developed a 4-degree-of-freedom (4-DOF) robotic dolphin with a horizontal caudal fin [4]. Yu *et al.* provided an active yaw and pitch control method for a multi-link dolphin robot to achieve agile and swift pitch maneuvers [5]. Cao *et al.* proposed a heading controller based on a self-tuning fuzzy strategy for a robotic dolphin to resolve a noticeable steady-state error [6]. An integrative control method depending on a combination of pitch, roll, yaw, and depth control strategies to achieve precise attitude control for dolphin leaping behavior was presented [7]. A depth controller combining sliding mode control (SMC) in conjunction with a fuzzy strategy on a robotic dolphin was also developed [8].

Though the maneuverability of robotic dolphins has been greatly developed, the limited endurance has always been a barrier for robotic dolphins, largely hampering their practical applications in oceans. By contrast, underwater gliders, as a long endurance underwater vehicle, have the ability to cruise for months and travel thousands of kilometers. The beginning of underwater gliders research can be traced back to last century. In 1989, Stommel published an article which firstly inspired gliding motion [9]. In the last decade, underwater gliders developed rapidly. The first generation of underwater gliders called "Spray" [10], "Seaglider" [11], and "Slocum" [12] were developed and tested in 2001. Besides, motion control and path planning for underwater gliders have also been developed, for instance, Nina *et al.* presented an approximate analytical expression as a planning strategy for energy efficient paths [13]. Furthermore, for the stabilization of underwater gliders, Zhang and Tan offered a method based on a passivity-based controller and a nonlinear model-based observer [14]. Moreover, a method was presented to estimate the under gliders' position by comparing two kinds of travel time [15]. However, neither speed nor maneuverability of underwater gliders is considerable. Therefore, with full consideration of both high maneuverability and long endurance, some researchers combined gliding motion with the basis of robotic dolphins to extend the duration. Wu *et al.* offered an innovative design for a gliding robotic dolphin, which achieved the basic swimming modes including the flapping and gliding motions. Moreover, they separately analyzed the hydrodynamic forces on the body, flippers, and flattened fluke while the robotic dolphin was gliding [16]. Yuan *et al.* developed a 1.5-m-long gliding robotic dolphin, and proposed a heading control method with the SMC based on the dynamic model for 3-D gliding motion [17].

In previous work, the study of gliding robotic dolphins emphasised on the platform development, but rarely involved its dynamic modeling. Therefore, on the basis of existing researches, a further progress is made in this paper, whose objective is to establish a complete dynamic model. Different from previous studies, we make the dynamic modeling with full consideration of both 3-D flapping and gliding motion. Furthermore, via simulations, this paper offers some comparison of the spiraling motion based on the two different swimming modes, accompanying with corresponding comparative analyses. Finally, we verify the complete dynamic model, and analyze the yaw angle and diving depth by comparing the

*This work was supported in part by the National Natural Science Foundation of China under Grant 61421004, Grant 61633020, Grant 61633017, Grant 61603388, and Grant 61725305, and in part by the Key Project of Frontier Science Research of Chinese Academy of Sciences (Grant No. QYZDJ-SSW-JSC004).

[1]J. Wang and Y. Yang are with the University of Chinese Academy of Sciences, Beijing 100049, China, {wangjian2016, yangyueqi2016}@ia.ac.cn

[2]J. Wang, Z. Wu, Y. Yang, M. Tan, and J. Yu are with the State Key Laboratory of Management and Control for Complex Systems, Institute of Automation, Chinese Academy of Sciences, Beijing 100190, China, {wangjian2016, zhengxing.wu, yangyueqi2016, min.tan, junzhi.yu}@ia.ac.cn

978-1-5386-6869-6/18/$31.00 © 2018 IEEE

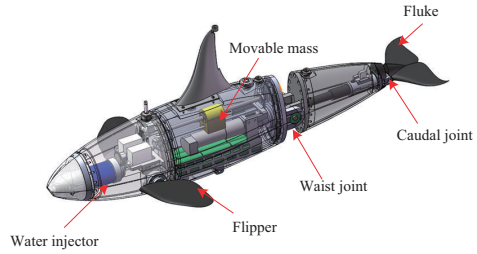

(a)

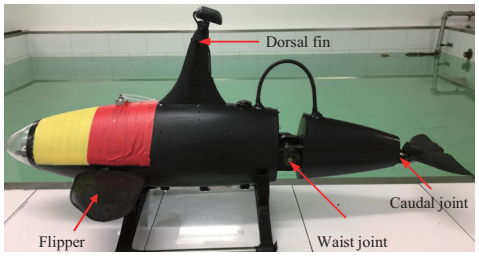

(b)

Fig. 1. Illustration of the gliding robotic dolphin. (a) Mechanical structure. (b) Prototype.

aquatic experiments with simulation.

The rest of this paper is organized as follows. In Section II, the mechanical design of a gliding robotic dolphin is offered. Section III provides detailed analyses in the complete dynamic model, which includes kinematic analysis and dynamic analysis. The experiments as well as simulation analyses are presented in Section IV. Finally, conclusions and future work are summarized in Section V.

II. Mechanical Design

The mechanical structure and prototype of the gliding robotic dolphin are illustrated in Fig. 1, which mainly includes the gliding part and dolphin-like swimming part. The gliding robotic dolphin is designed as a killer whale. The total mass and length of the gliding robotic dolphin are 9.1 kg and 0.83 m, respectively.

A. Structure About the Gliding Motion

The key design that allows the robotic dolphin to glide is the buoyancy-driven system, which regulates surfacing and diving by adjusting the buoyancy. In this paper, the buoyancy-driven system is mainly composed of a water injector and a piston. With the movement of the piston, water is drawn into or drained out of the water injector, which directly leads to the reduction or increase in the overall volume, further increases or reduces the buoyancy of robotic dolphin. Besides, since the capacity of the water injector is a constant, the total volume determines not only the upper limit of net buoyancy, but also the maximum gliding speed.

Another key design is the movable mass, which can be used alone to adjust the pitch angle of the gliding robotic dolphin. Moreover, combining with the flippers or fluke, it achieves decoupling control of pitch angle and gliding angle.

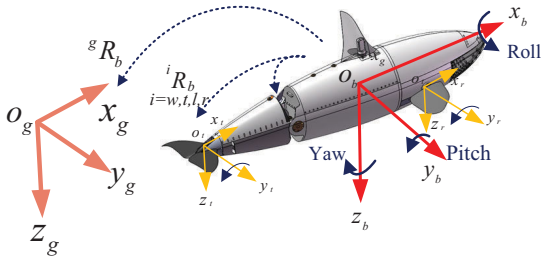

Fig. 2. Coordinate systems including inertial, body, and fin frames.

B. Structure of the Flapping Motion

The dolphin-like swimming part consists of a waist joint, a tail joint, and two flippers joints. The waist and tail joints of the gliding robotic dolphin yield the main thrust for flapping motion. Additionally, the two flippers can generate lift force or attitude adjustment during gliding motions, which is a unique feature compared with the conventional underwater gliders.

III. Dynamic Modeling for the Gliding Robotic Dolphin

To clearly describe a complete dynamic model of the gliding robotic dolphin, coordinate systems including an inertial frame, a body-fixed frame, a waist frame, a tail frame, and two flippers frames are defined firstly. All the coordinate frames are illustrated in Fig. 2, and these frames follow the right-hand rule. Moreover, we denote the inertia frame $C_g = o_g x_g y_g z_g$, the z axis of which is along the direction of gravity, while the x and y are perpendicular to z. Next, we define a body-fixed frame $C_b = o_b x_b y_b z_b$, the origin of which locates at the center of buoyancy (CB). In particular, $C_w = o_w x_w y_w z_w$, $C_t = o_t x_t y_t z_t$, $C_l = o_l x_l y_l z_l$, and $C_r = o_r x_r y_r z_r$ represent the joint frames of waist, tail, left flipper, and right flipper, respectively. Furthermore, we define $\boldsymbol{j} = [0,1,0]^T$, $\boldsymbol{k} = [0,0,1]^T$, and $\boldsymbol{J} = [0_{1\times 3}, \boldsymbol{j}]^T$. Finally, for two vectors $\boldsymbol{p}, \boldsymbol{q} \in R^3$, their cross product is denoted as $\boldsymbol{p} \times \boldsymbol{q} = \hat{\boldsymbol{p}} \cdot \boldsymbol{q}$ where $\hat{\boldsymbol{p}}$ represents the skew matrix of $\boldsymbol{p}$.

A. Kinematic Analysis

Denote $U_b = (U_{bx}, U_{by}, U_{bz})^T$ and $\Omega_b = (\Omega_{bx}, \Omega_{by}, \Omega_{bz})^T$ the line velocity and angular velocity of the gliding robotic dolphin with respect to (w.r.t.) the body frame, respectively. Therefore, $V_b = ({U_b}^T, {\Omega_b}^T)^T$ denotes the velocity vector. The kinematics of the robot are formalized by

$$\begin{aligned} {}^g\dot{P}_b &= {}^gU_b = {}^gR_b U_b \\ {}^g\dot{R}_b &= {}^gR_b \hat{\Omega}_b \end{aligned} \tag{1}$$

where ${}^gR_b$ and ${}^gP_b$ denote the rotation matrix and position vector of C_b w.r.t. C_g, and ${}^gR_b$ is determined by roll angle ψ, pitch angle θ, and yaw angle φ.

Afterwards, since the surfaces driven by flipper joints, waist joint, and tail joint are movable, we should consider

their offset angles for their kinematics

$$\begin{aligned} V_i &= {}^iH_bV_b + \delta_i \qquad (i = w,l,r) \\ V_t &= {}^tH_wV_w + \delta_t \end{aligned} \tag{2}$$

where

$${}^iH_b = {}^bH_i{}^T = \begin{pmatrix} {}^iR_b & -{}^iR_b{}^b\hat{P}_i \\ 0_{3\times3} & {}^iR_b \end{pmatrix} \quad (i = w,l,r)$$

$${}^tH_w = {}^wH_t{}^T = \begin{pmatrix} {}^tR_w & -{}^tR_w{}^w\hat{P}_t \\ 0_{3\times3} & {}^tR_w \end{pmatrix}$$

$$\delta_i = \dot{\theta}_iJ_i \quad (i = w,t,l,r)$$

The indexes b, w, t, l, r correspond to the body, waist, tail, left flipper, and right flipper. δ_i indicates the speed change caused by fin surface's movements. ${}^bP_i(i = w,l,r)$ represents a corresponding position vector, and ${}^iR_b(i = w,l,r)$ indicates the rotation matrix from coordinate frame C_b to C_i, which is related to offset angle θ_i of movable surfaces w.r.t. frame C_b.

$${}^iR_b = {}^bR_i{}^T = \begin{pmatrix} \cos\theta_i & 0 & -\sin\theta_i \\ 0 & 1 & 0 \\ \sin\theta_i & 0 & \cos\theta_i \end{pmatrix}$$

Regarding the rotation matrix and position vectors from frame C_w to C_t, there exists the same form and meaning.

B. Net Buoyancy Analysis

One of main external forces is the net buoyancy that represents the difference between gravity and buoyancy [17]. When the position of the piston is at the middle point of water injector, the net buoyancy is zero. Therefore, the net buoyancy of the robot w.r.t. frame C_b is given by

$$G_n = \rho S(\frac{h_o}{2} - h)g({}^gR_b{}^Tk) \tag{3}$$

where ρ indicates the density of the water; g denotes the gravitational acceleration; S and h_o indicate the bottom area and the total height of the water injector, respectively; h denotes the real position of piston. Hence, the moment of net buoyancy take the forms as follows

$$\tau_n = (m_b\hat{P}_b + m_j\hat{P}_j + m_m\hat{P}_m)g({}^gR_b{}^Tk) + G_n\hat{P}_{in} \tag{4}$$

where m_b is the body's mass excluding the movable and water injector mass; m_m and m_j denotes the movable and water injector mass; P_b, P_m, and P_j are the position vectors of corresponding center of gravity (CG) w.r.t. frame C_b; P_{in} indicates the movable vector of CG caused by the movement of piston. Hence, we define $G_b = (G_n, \tau_n)^T$.

C. Hydrodynamic Analysis

Hydrodynamics is another major external forces of robotic dolphins, which is analyzed with the quasi-steady model in this paper [17], [18]. Hydrodynamic is closely related to the relative attitude which can be parameterized by the angle of attack α_i and the sideslip angle $\beta_i(i = b,w,t,l,r)$. For convenience, we introduce a velocity coordinate frame $C_v = o_vx_vy_vz_v$ to characterize the relative attitude. Therefore, the hydrodynamic forces of body and movable surfaces and their moments can be calculated by

$$\begin{aligned} {}^vF_i &= \begin{pmatrix} -{}^vD_i \\ {}^vSF_i \\ -{}^vL_i \end{pmatrix} = \tfrac{1}{2}\rho S_iU_i{}^2 \begin{pmatrix} -C_{i,d}(\alpha_i) \\ C_{i,sf}(\beta_i) \\ -C_{i,l}(\beta_i) \end{pmatrix} \\ {}^v\tau_b &= \begin{pmatrix} {}^v\tau_{ix} \\ {}^v\tau_{iy} \\ {}^v\tau_{iz} \end{pmatrix} = \tfrac{1}{2}\rho S_iU_i{}^2 \begin{pmatrix} C_{i,\tau x}(\beta_i) \\ C_{i,\tau y}(\alpha_i) \\ C_{i,\tau z}(\beta_i) \end{pmatrix} + K_i\Omega_i \end{aligned} \tag{5}$$

where S_i presents the reference area of body and movable surfaces; C indicates the corresponding hydrodynamic coefficients related to the angle of attack and the sideslip angle; K_i denotes the matrix of the rotating damping coefficients.

Next, since the forces of body and movable surfaces are expressed in the velocity coordinate frame, it is necessary to transform them to their own coordinate frames with The rotation matrix ${}^iR_v$. Furthermore, we unify all the physical quantities into the body coordinate frame

$$\begin{pmatrix} {}^bF_i \\ {}^b\tau_i \end{pmatrix} = \begin{pmatrix} {}^bR_i & 0_{3\times3} \\ {}^b\hat{P}_i{}^bR_i & {}^bR_i \end{pmatrix} \begin{pmatrix} {}^iR_v{}^vF_i \\ {}^iR_v{}^v\tau_i \end{pmatrix} \tag{6}$$

where $i = b,w,t,l,r$, ${}^bR_b = I_{3\times3}$, and ${}^b\hat{P}_b = 0_{3\times3}$.

D. Dynamic Model

For five coordinate frames including body, waist joint, tail joint, right flipper, and left flipper frames, their own dynamic models can be derived as follows by Newton's law

$$\begin{aligned} M_b\dot{V}_b &= -F_{cb} + F_{hb} + F_{wb} + F_{lb} + F_{rb} + G_b + \Gamma_m + \Gamma_j \\ {}^bH_wM_w\dot{V}_w &= {}^bH_w(-F_{cw} + F_{hw} + F_{bw} + \mathrm{F}_{tw}) \\ {}^bH_tM_t\dot{V}_t &= {}^bH_t(-F_{ct} + F_{ht} + F_{wt}) \\ {}^bH_lM_l\dot{V}_l &= {}^bH_l(-F_{cl} + F_{hl} + F_{bl}) \\ {}^bH_rM_r\dot{V}_r &= {}^bH_r(-F_{cr} + F_{hr} + F_{br}) \end{aligned} \tag{7}$$

where $M_i(i = b,w,t,l,r)$ represents the total inertia matrix; Γ_m and Γ_j denote the forces of movable mass and water injector on body; $F_{ci} = (f_{ci}, \tau_{ci})^T(i = b,w,t,l,r)$ denotes Coriolis force and moment on part i; $F_{hi} = (f_{hi}, \tau_{hi})^T(i = b,w,t,l,r)$ denotes hydrodynamic force and moment on part i; $F_{bi} = (f_{bi}, \tau_{bi})^T(i = w,l,r)$ indicates the external force of body on part i; On the contrary, $F_{ib} = (f_{ib}, \tau_{ib})^T$ expresses the external force of part i on body, and the same explanation for F_{wt} or F_{tw}. The purpose of multiplying both sides of the equation by ${}^bH_i$ is to transform the forces and moments from joints frame to body frame. Thereby, it follows that ${}^bH_iF_{bi} + F_{ib} = 0$ since they are the interaction forces.

Afterwards, (2) formalizes the kinematic of body and movable surfaces, so we can derive the basic form of each speed derivative

$$\begin{aligned} \dot{V}_i &= {}^i\dot{H}_bV_b + {}^iH_b\dot{V}_b + \dot{\delta}_i \qquad (i = w,l,r) \\ \dot{V}_t &= {}^t\dot{H}_wV_w + {}^tH_w\dot{V}_w + \dot{\delta}_t \end{aligned} \tag{8}$$

where

$${}^i\dot{H}_b = \begin{pmatrix} -\dot{\theta}_i\hat{j}_i{}^iR_b & \dot{\theta}_i\hat{j}_i{}^iR_b{}^b\hat{P}_i \\ 0_{3\times3} & -\dot{\theta}_i\hat{j}_i{}^iR_b \end{pmatrix} \qquad (i = w,l,r)$$

Move one step further, in order to make the equation more concise, two variables by the following forms are defined

$$\xi_t = {}^t\dot{H}_w V_w \quad \text{and} \quad \xi_i = {}^i\dot{H}_b V_b \quad (i = w,l,r)$$

Therefore, the final form can be obtained

$$\begin{aligned} \dot{V}_i &= {}^iH_b\dot{V}_b + \xi_i + \dot{\delta}_i \qquad (i = w,l,r) \\ \dot{V}_t &= {}^tH_b\dot{V}_b + {}^tH_w(\xi_w + \dot{\delta}_w) + \xi_t + \dot{\delta}_t \end{aligned} \tag{9}$$

where ${}^tH_b = {}^tH_w{}^wH_b$. Hence, by substituting (9) into the left sides of (7) and add the left sides of (7), we can derive

$$\sum_{i=b,w,t,l,r} {}^bH_iM_i\dot{V}_i = (\sum_{i=b,w,t,l,r} {}^bH_iM_i{}^iH_b)\dot{V}_b + \Pi_e \tag{10}$$

where

$$\Pi_e = \sum_{i=b,w,t,l,r} {}^bH_iM_i(\xi_i + \dot{\delta}_i) + {}^bH_tM_t{}^tH_w(\xi_w + \dot{\delta}_w)$$

Similarly, the sum of all forces and moments by adding the right sides of (7) can be derived. Furthermore, according to the equality of the left and right sides of the equation, the final kinetic equation can be taken as the following forms

$$M\dot{V}_b = -\Pi_e + \Pi_c + \Pi_h + \Pi_g + \Gamma_m + \Gamma_j \tag{11}$$

where

$$M = \sum_{i=b,w,t,l,r} {}^bH_iM_i{}^iH_b$$

$$\Pi_c = -\sum_{i=b,w,t,l,r} {}^bH_iF_{ci} = -\sum {}^bH_i \begin{pmatrix} \hat{\Omega}_i & 0_{3\times3} \\ \hat{V}_i & \hat{\Omega}_i \end{pmatrix} M_i \begin{pmatrix} V_i \\ \Omega_i \end{pmatrix}$$

$$\Pi_h = \sum_{i=b,w,t,l,r} {}^bH_iF_{hi}$$

$$\Pi_g = G_b$$

$$\Gamma_m = m_m \begin{pmatrix} 2\hat{\dot{P}}_m\Omega_b - \ddot{P}_m \\ \hat{P}_m(2\hat{\dot{P}}_m\Omega_b - \ddot{P}_m) \end{pmatrix}$$

$$\Gamma_j = m_j \begin{pmatrix} 2\hat{\dot{P}}_j\Omega_b - \ddot{P}_j \\ \hat{P}_j(2\hat{\dot{P}}_j\Omega_b - \ddot{P}_j) \end{pmatrix}$$

It is assumed that $\ddot{P}_m = \ddot{P}_j = 0_{3\times1}$ since the instantaneous acceleration and deceleration processes of the piston and movable mass are rapid enough. Regarding the $\dot{P}_m$ and $\dot{P}_j$, we can derive them from movable mass's speed U_m and piston's speed U_j, respectively

$$\begin{aligned} \dot{P}_m &= U_m \\ \dot{P}_j &= U_j \end{aligned} \tag{12}$$

where P_{m0} and P_{j0} denote the initial position of the movable mass and the piston, respectively. Furthermore, M_i is sum of the inertia matrix of the robot M_{di} and the added inertia matrix M_{adi} from the surrounding water.

$$M_{di} = \begin{pmatrix} m_iI_{3\times3} & \left(m_i\hat{P}_i\right)^T \\ m_i\hat{P}_i & J_i \end{pmatrix} \qquad (i = w,t,l,r)$$

$$M_{db} = \begin{pmatrix} (m_b + m_m + m_j)I_{3\times3} & \left(\sum_{i=b,j,m} m_i\hat{P}_i\right)^T \\ \left(\sum_{i=b,j,m} m_i\hat{P}_i\right) & J_b - \sum_{i=b,j,m} m_i\hat{P}_i\hat{P}_i \end{pmatrix}$$

where $J_i (i = b,w,t,l,r)$ represents the rotational inertial caused by the distribution of m_i, and it is relative to its CG.

TABLE I. Parameters of dynamic model

Parameter	Value	Parameter	Value
m_b	5.28 kg	${}^bP_w$	$[-0.2257, 0, -0.0123]^T$
m_w	0.5 kg	${}^bP_t$	$[-0.4488, 0, -0.0123]^T$
m_t	0.077 kg	${}^bP_l$	$[0.1063, -0.0615, 0.0318]^T$
$m_l(m_r)$	0.074 kg	${}^bP_r$	$[0.1063, 0.0615, 0.0318]^T$
m_m	0.42 kg	J_w	$diag\{0.0004, 0.0026, 0.0023\}$
m_j	0.035 kg	J_t	$diag\{0.0001, 0, 0.0001\}$
g	9.8 m/s^2	$J_l(J_r)$	$diag\{0.0001, 0, 0.0001\}$
ρ	998.2 kg/m^3	P_l	$[-0.014, -0.05923, 0]^T$
P_w	$[-0.109, 0, 0]^T$	P_r	$[-0.014, 0.05923, 0]^T$
P_t	$[-0.041, 0, 0]^T$	P_b	$[0.001, 0, 0.052]^T$
P_{j0}	$[0.1953, 0, 0]^T$	P_{m0}	$[-0.04077, 0, -0.03715]^T$

IV. Results and Analyses

In this paper, we analyze the steady state spiraling motion based on two motions which include the flapping and gliding motions. By simulation, we can draw some conclusions about the two motions. Subsequently, extensive aquatic experiments were carried out to verify the built dynamic model in a 2.4 m depth diving pool.

A. Simulation Results

MATLAB SIMULINK is used to implement the simulations to verify the validity of the complete dynamic model. Firstly, some physical parameters of dynamic model are tabulated in Table I. Furthermore, hydrodynamic parameters are computed using both computational fluid dynamics (CFD) software packages and the curve fitting method [19], and then some appropriate adjustments based on experiences are made. Finally, we can get the rotational inertia of body and movable surfaces by measuring quality property in SolidWorks. It should be noted that J_w, J_t, J_l, and J_r are diagonal matrix, which are listed in Table I.

$$J_b = \begin{pmatrix} 0.0158 & 0 & 0.0029 \\ 0 & 0.1699 & 0 \\ 0.0029 & 0 & 0.1678 \end{pmatrix}$$

- In the flapping motion, the maximum joint amplitudes of the waist, tail, and phase between them are set at 30°, 45°, and 35°, respectively, and the frequency is 2 Hz. Simultaneously, the offset angles of left flipper and right flipper are $-45°$ and 0°. Figs. 3(a) denotes 3-D trajectory within 50 s. We could see the robot only dives to the depth of 5.7 m, and its turning radius is nearly 3 m.
- In the gliding motion, we let the movable mass move forward 150 cm, and the piston move backward 5.25 cm. The offset angle of left flipper and right flipper are same as the flapping motion. Figs. 3(b) illustrates 3-D trajectory within 50 s. The diving depth and turning radius in the motion are 8.7 m and less than 1 m.

In terms of spiraling movement, gliding mode or flapping mode, asymmetric hydrodynamic that would produce

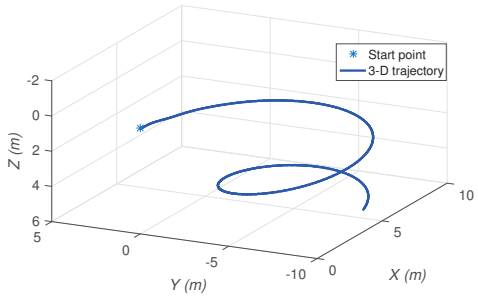

(a)

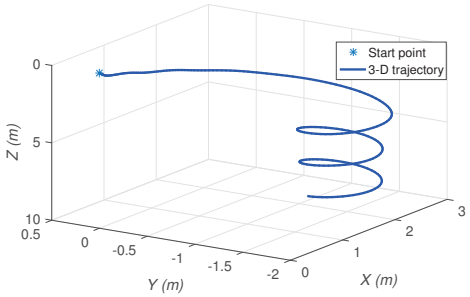

(b)

Fig. 3. 3-D trajectory of spiraling movements. (a) Flapping motion. (b) Gliding motion.

Fig. 4. Snapshot sequence in gliding motion.

steering yaw moment can be generated in the left and right sides of the body through the difference of flipper fins. The following rolling motion causes the lift and drag forces in the vertical plane, which makes the body roll. On the other hand, the horizontal components of the two forces generate a centripetal force for the steady state spiraling movement. Thus, the projection of the steady 3-D trajectory of Fig. 3 on the horizontal plane is circular.

B. Experimental Results

Experiments are implemented to validate the spiraling motion of the gliding robot in a 2.4 m depth diving pool. The snapshot sequences of the spiraling motion in gliding motion and flapping motion are shown in Figs. 4 and 5.

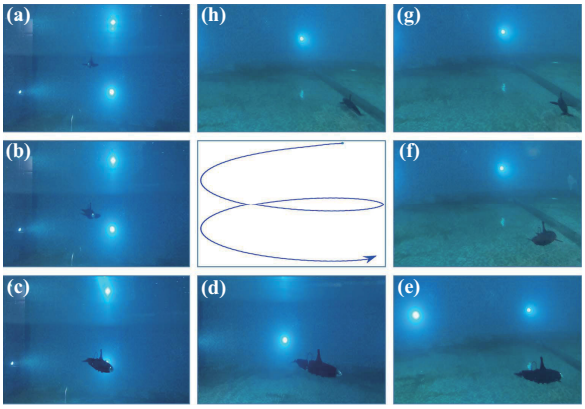

Fig. 5. Snapshot sequence in flapping motion.

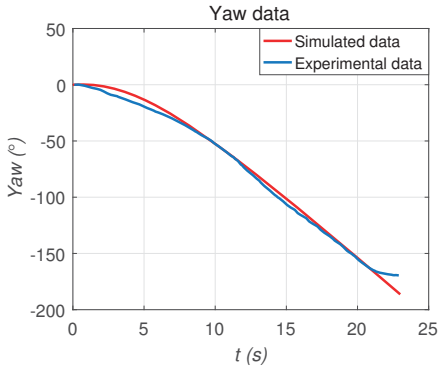

(a)

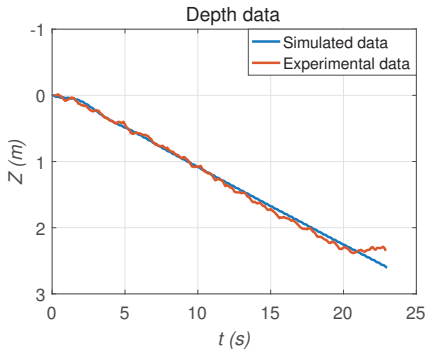

(b)

Fig. 6. The simulated and experimental results in flapping motion: (a) Yaw angle; (b) Diving depth.

Besides, in gliding motion, due to the limited depth, we set the movable mass and piston at target positions which are same as simulation before diving.

From Figs. 6 and 7, regarding the yaw angle and diving depth, the experimental data is consistent with the simulation shape, which signifies that the 3-D completed dynamic model is valid. Furthermore, some conclusions can be drawn via comparing spiraling movements of the gliding and flapping motion. Firstly, the diving depth in the gliding motion is greater than flapping motion within the same time, for both the flipper fins and movable mass can supply the pitch

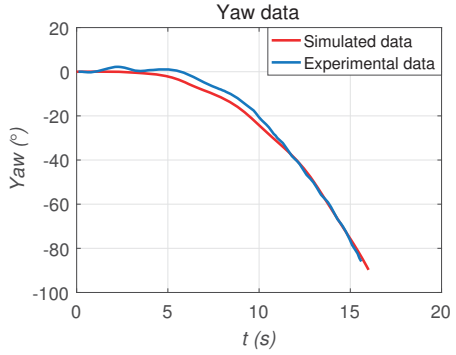

(a)

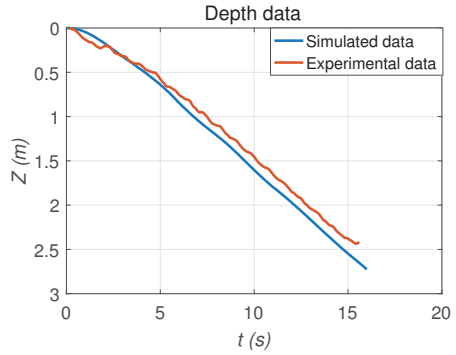

(b)

Fig. 7. The simulated and experimental results in gliding motion. (a) Yaw angle. (b) Diving depth.

moment in the spiraling movement, the latter of which brings about a higher effect. Moreover, since the net buoyancy effect has a certain delay, the diving speed in flapping motion is faster than gliding in the early diving state, which directly the change of yaw angle in the flapping motion is greater than that of the gliding motion. However, when the body posture in gliding motion comes to a stable state, the gliding robotic dolphin could achieve a bigger diving speed, which could offer a smaller turning radius. On the contrary, due to the dorsoventral propulsive mechanism, the robot has a relatively stable forward speed, which results in a stable change in the yaw angle. However, since the yaw moment in flapping is smaller than gliding motion in the late stage, the turning radius is much bigger.

V. Conclusions and Future Work

In this paper, we have proposed a complete dynamic model with full consideration of both 3-D gliding motion and flapping motion for the gliding robotic dolphin, and provided detailed derivation process. By simulations based on the complete dynamic model, difference of spiraling movements in the flapping motion and gliding motion was compared. Via aquatic experiments, we analyzed the characteristics of spiraling movement including the yaw angle and diving depth, further proved the dynamic model is effective. In contrast, we can conclude that spiraling movement in the gliding motion is more stable and energy efficient than in the flapping motion.

In the future, we plan to conduct underwater fixed depth, fixed direction, and tracking control based on the model, and compare the difference between the two swimming motions through aquatic experiments. We will also make some engineering research according to practical underwater applications of gliding robotic dolphins.

References

[1] F. E. Fish and J. J. Rohr, "Review of dolphin hydrodynamics and swimming performance," U.S. Navy, San Diego, CA, *Tech. Rep. 1801*, Aug. 1999.

[2] M. Nagai, *Thinking Fluid Dynamics with Dolphins*. Tokyo, Japan: Ohmsha, 2002.

[3] M. Nakashima, T. Tsubaki, and K. Ono, "Three-dimensional movement in water of the dolphin robot–Control between two positions by roll and pitch combination," *J. Robot. Mechatronics*, vol. 18, no. 3, pp. 347–355, 2006.

[4] G. Dogangil, E. Ozcicek, and A. Kuzucu, "Modeling, simulation, and development of a robotic dolphin prototype," in *Proc. IEEE Int. Conf. Mechatronics Autom.*, Canada, Jul. 2005, pp. 952–957.

[5] J. Yu, Z. Su, M. Wang, M. Tan, and J. Zhang, "Control of yaw and pitch maneuvers of a multilink dolphin robot," *IEEE Trans. Robot.*, vol. 28, no. 2, pp. 318–329, 2012.

[6] Z. Cao, F. Shen, C. Zhou, N. Gu, S. Nahavandi, and D. Xu, "Heading control for a robotic dolphin based on a self-tuning fuzzy strategy," *Int. J. Adv. Robot. Syst.*, vol. 13, no. 28, pp. 1–8, 2016.

[7] J. Yu, Z. Su, Z. Wu, and M. Tan, "An integrative control method for bio-inspired dolphin leaping: Design and experiments," *IEEE Trans. Ind. Electron.*, vol. 63, no. 5, pp. 3108–3116, 2016.

[8] J. Yu, J. Liu, Z. Wu, and F. Hao, "Depth control of a bioinspired robotic dolphin based on sliding mode fuzzy control method," *IEEE Trans. Ind. Electron.*, vol. 65, no. 3, pp. 2429–2438, 2018.

[9] H. Stommel, "The slocum mission," *Oceanography*, vol. 2, no. 1, pp. 22–25, 1989.

[10] J. Sherman, R. E. Davis, W. B. Owens, and J. Valdes, "The autonomous underwater glider 'Spray'," *IEEE J. Ocean. Eng.*, vol. 26, no. 4, pp. 437–446, 2001.

[11] C. C. Eriksen, T. J. Osse, R. D. Light, T. Wen, T. W. Lehman, P. L. Sabin, J. W. Ballard, and A. M. Chiodi, "Seaglider: A long-range autonomous underwater vehicle for oceanographic research," *IEEE J. Ocean. Eng.*, vol. 26, no. 4, pp. 424–436, 2001.

[12] D. C. Webb, P. J. Simonetti, and C. P. Jones, "SLOCUM: An underwater glider propelled by environmental energy," *IEEE J. Ocean. Eng.*, vol. 26, no. 4, pp. 447–452, 2001.

[13] N. Mahmoudian, J. Geisbert, and C. Woolsey, "Approximate analytical turning conditions for underwater gliders: Implications for motion control and path planning," *IEEE J. Ocean. Eng.*, vol. 35, no. 1, pp. 131–143, 2010.

[14] F. Zhang and X. Tan, "Passivity-based stabilization of underwater gliders with a control surface," *J. Dyn. Syst. Meas. Control.*, vol. 137, no. 6, p. 061006 (13 pp), 2015.

[15] J. Sun, S. Liu, J. Yu, A. Zhang, and F. Zhang, "Localization of underwater gliders with acoustic travel-time in an observation network," in *Proc. IEEE Oceanic Eng. Society*, Shanghai, China, Apr. 2016, pp. 1–5.

[16] Z. Wu, J. Yu, J. Yuan, M. Tan, and J. Zhang, "Mechatronic design and implementation of a novel gliding robotic dolphin," in *Proc. IEEE Int. Conf. Robot. Biomim.*, Zhuhai, China, Dec. 2015, pp. 267–272.

[17] J. Yuan, Z. Wu, J. Yu, and M. Tan, "Sliding mode observer-based heading control for a gliding robotic dolphin," *IEEE Trans. Ind. Electron.*, vol. 64, no. 8, pp. 6815–6824, 2017.

[18] J. G. Graver, "Underwater gliders: Dynamics, control, and design," Ph.D. dissertation, Dept. Mech. Aerosp. Eng., Princeton Univ., Princeton, NJ, 2005.

[19] J. Yu, J. Yuan, Z. Wu, and M. Tan, "Data-driven dynamic modeling for a swimming robotic fish," *IEEE Trans. Ind. Electron.*, vol. 63, no. 9, pp. 5632–5640, 2016.